Assessment of Shell Strength During Solidification in the Mold Cracking Simulator (MCS) Test

BEGOÑA SANTILLANA, VAMSI PARUCHURI, VIKTOR KRIPAK, ULRICH PRAHL, and CAREL TEN HORN

To properly model the cracking susceptibility during solidification under continuous casting conditions, it is essential to have accurate data. Such data for the mechanical properties of steel during solidification are scarce if not non-existent. An experimental tool called the Mold Cracking Simulator (MCS) has been used to simulate the initial shell formation under continuous casting conditions. As part of the test, the shell is mechanically subjected to deformation. A mathematical model has been developed to translate the force and elongation measured during the MCS trials into stress–strain components. To test the model and validate the assumptions, two steel grades were tested, a peritectic steel grade and a higher-alloyed grade. The results show that the reproducibility of the test is very good and the stress–strain curves are consistent with the steel composition. Moreover, the metallographic and fractographic analysis of the deformed MCS samples shows that the microstructure is comparable to that of a continuously cast product and the cracks generated are interdendritic, *i.e.*, hot tears.

https://doi.org/10.1007/s11661-018-4958-8

I. INTRODUCTION

THE continuous trend towards improving casting productivity by increasing casting speed in combination with higher-quality demands for defect-free products and development of new high-alloyed steel grades demands an understanding of the thermomechanical properties of steels during solidification.

Nowadays, modeling has become widely available and has led to significant improvement in product quality and process performance. However, models require accurate input data but often mechanical properties are scarce or even non-existent at temperatures in the solidification range of steel alloys of commercial interest.[1]

Material properties are inherent to each steel composition, and many methods have been used to measure material properties at different temperatures.[2–14] Several methods are available to assess the material strength in the solidification region, but few include the influence of casting process parameters. Many of these methods are standard mechanical tests such as tensile, torsion, or bending tests, where the samples are reheated to temperature above liquidus, cooled to the test temperature and deformed.

Because the original microstructure during solidification differs from reheated samples, better *in situ* testing methods were developed to measure the mechanical properties of metal during solidification. One such testing method is the Submerged Split Chill Tensile (SSCT) test first introduced in 1985 by Ackermann *et al.*[15] for testing aluminum, which was later updated to include steels.[6,7,16] However, SSCT has a disadvantage being a static model, meaning that the device is not capable of simulating the dynamics of a continuous casting process, particularly the oscillation cycles and mold slag penetration. In this regard, the "Mold Crack Simulator" MCS[17] developed in 2010 can mimic most of the dynamics of continuous casting as well as measuring the strength of different steels during solidification. Recently Wang *et al.* have also developed a Mold Cracking simulator at the Central South University, China,[14] with the purpose of studying the dynamics of shell tearing during solidification.

BEGOÑA SANTILLANA is with the Steelmaking & Casting Group, Ironmaking, Steelmaking & Casting Department, Tata Steel, Research & Development, IJmuiden Technology Centre, P.O. Box 10000, 1970 CA, IJmuiden, The Netherlands. Contact e-mail: begona.santillana@tatasteeleurope.com VAMSI PARUCHURI is with the RWTH Aachen University, Aachen, Germany and also with the Department Materials Science and Engineering, TU Delft/Faculteit 3mE, Gebouw 34, Mekelweg 2, 2628 CD, Delft, The Netherlands. VIKTOR KRIPAK is with the Institut für Eisenhüttenkunde (IEHK), RWTH Aachen, Aachen, Germany. ULRICH PRAHL is with the Institut für Eisenhüttenkunde (IEHK), RWTH Aachen and also with the Technische Universität Bergakademie Freiberg, Institut für Metallformung, Bernhard-von-Cotta-Str. 4, 09599 Freiberg, Germany. CAREL TEN HORN is with the Plasticity & Tribology Group, Application & Engineering Department, Tata Steel, Research & Development, IJmuiden Technology Centre, 1970 CA, IJmuiden, The Netherlands.

Manuscript submitted November 3, 2017.
Article published online October 30, 2018

However, to quantitatively compare data for different material compositions or even the influence of different process parameters in a material solidification, a proper methodology is necessary that provides basic design information on the strength of a material.[18] The engineering tension test does not give a true indication of the deformation characteristics of a material because it is based on the original dimensions of the sample tested which change continuously during testing. For this reason a flow curve represents better the plastic-flow characteristics of the material.[18] In this publication, a model is described to convert the raw data obtained from the MCS test to true stress–true strain flow curves.

II. TESTING PROCEDURE WITH THE MCS

In the MCS, the cylindrical mold is immersed into the liquid metal until the steel cap is fully submerged. After 5 Sec of freezing time a scull is formed around the cap, which further acts like a dummy bar as in the continuous caster to pull down the shell. Simultaneously, the mold tube is oscillated with an amplitude S of 3.5 mm and frequency f of 2 Hz. Consecutively, the cap moves downwards with a speed of 20 mm/s as an analogy of the casting speed in a continuous caster. The internal cooling block is tightly fitted in the mold and internal water-cooled provides indirect cooling to the copper mold. This indirect cooling system is chosen to reduce the risk of water leakage during the mechanical testing step, considering that the mechanical part of the test should be allowed to work even inside the liquid metal.

After ten oscillation cycles, a solidified shell of about 10 cm is formed and the whole system is ejected from the liquid steel bath. Due to strict safety precautions, deformation is performed outside of the melt bath. As soon as the oscillation is stopped, the hydraulic system is opened and the cooling block is pulled upwards. Consequently, due to sliding action between the wedge and cooling block, the wedge moves outwards pushing the shell in the radial direction. The signals recorded during the experiment are shown in Figure 1.

As shown in Figure 1, the recorded signals needed for the mechanical assessment are in the form of load and displacement; therefore, a mathematical model is needed to calculate the stress and strain from the data acquired.

The load applied in the radial direction by the wedge pushing the shell causes circumferential stress on the solidifying shell and tensile stress between dendrites, perpendicular to their main growth direction, as experienced in the continuous casting process (Figure 2).

Two thermocouples are positioned on the opposite side of the half-ring, embedded in the copper tube-mold (see Figure 3, left). Their signals shows a slight increase in temperature at the start of the loading procedure (see Figure 3, right). This is coherent with the fact that the shell is pulled away from the copper mold on the opposite side by the wedge. As a result, it is pushed to the mold where the thermocouples are located, increasing the contact with the mold surface. As the thermocouples are positioned at the mold surface, the maximum temperature values recorded by the upper thermocouple are consistent with the 600 °C to 800 °C expected values from the surface of a continuous casting mold.[19,20] These temperatures are slightly higher than actually measured in industrial casters but this is mainly due to the indirect cooling of the MCS and because the thermocouples do not really measure the copper temperature, but in fact what is measured is the temperature at the gap between the steel shell and the mold.

In the past, some attempts were made to measure the actual shell temperature during testing without success due to the dynamics of the parts. It is planned that in the future a thermal imaging camera will be used to measure the temperature at the steel shell.

III. MATHEMATICAL MODELING APPROACH

The mold cracking simulator has been designed with a cylindrical geometry in order to avoid complex 3D heat transfer effects. Since there are no sharp corners, the steel shell formed will have the same process parameters around its circumference. Moreover, a cylindrical shape

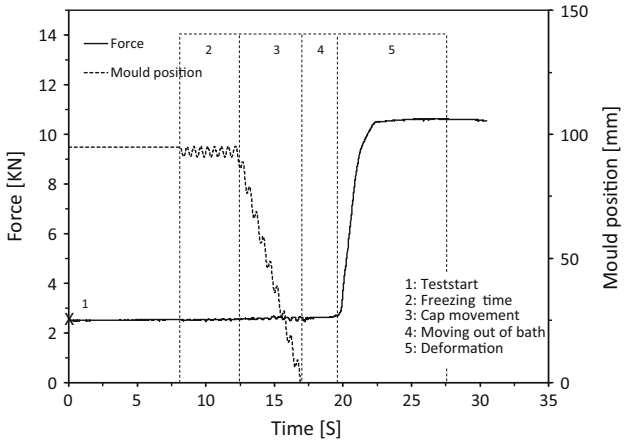

Fig. 1—Signals recorded during the Mold Crack Simulator experiment.

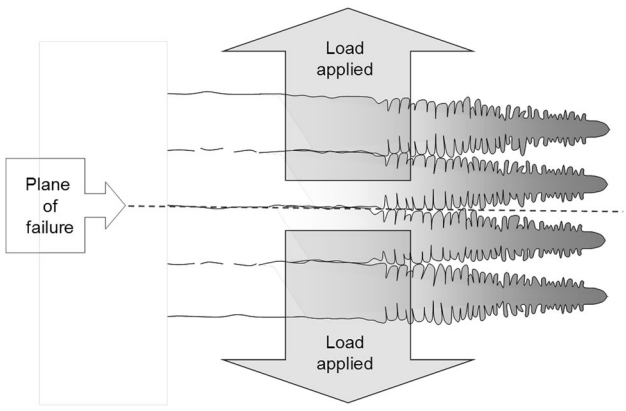

Fig. 2—Schematic representation of deformation between the dendrites.

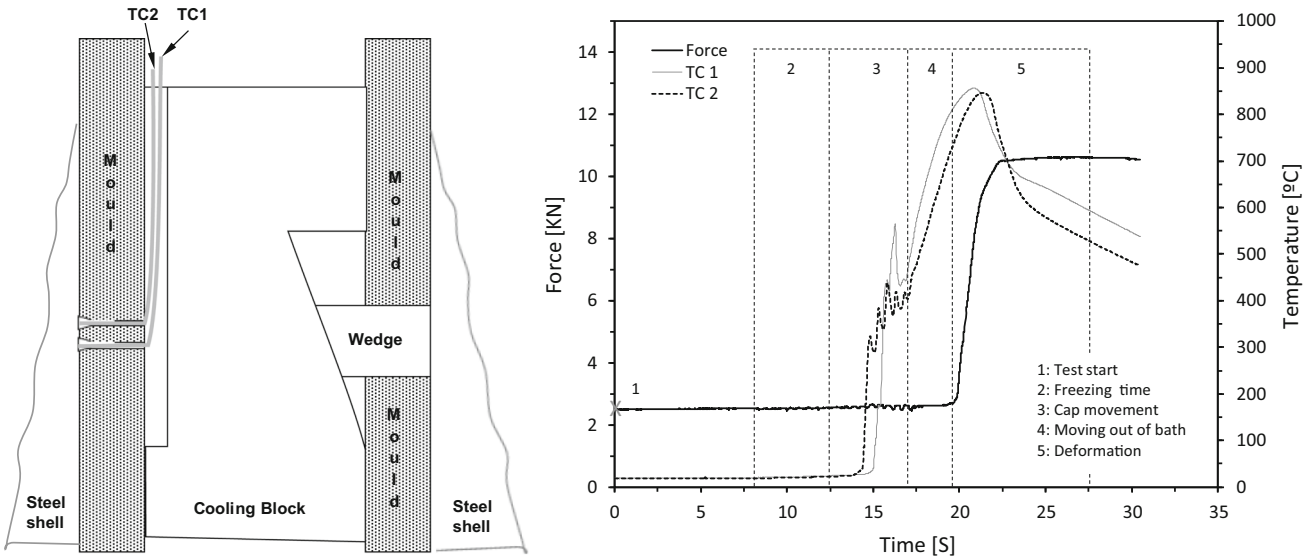

Fig. 3—Left: schematic representation of the thermocouple's position. Right: thermocouple signals recorded during testing, 1st test steel-2.

can be easily modeled using cylindrical coordinates, or in this case an analogy can be found between the MCS and bodies of annular cross section like pressure vessels.

Considering that the MCS is a circular cylindrical body of annular cross section subjected to surface forces and thermal loads, the present scenario of deformation is similar to that of "Pressure Vessels"[21] where a cylinder is subjected to internal pressure by the fluid flowing through it; the analogy in the MCS is that the wedge exerts internal pressure on the solidifying shell. Moreover, in both cases, the force applied in the radial direction of the cylinder is transformed into circumferential stress.

According to the equations governing the stress state, circular cylinders are divided into two groups[21]:

– The thin wall: when the wall thickness is small compared to the inside radius (when, $R/w \gg 1$) (R: Vessel Radius, w: wall thickness)
– The thick wall: (when, $R/w \ll 1$).

In the current work, the thin wall condition has been assumed since the wall thickness w is very small compared to the other dimensions of the shell and the inside radius (R (34.68 mm)/t (6 mm) $\gg 1$). This implies that the circumferential stress across the wall thickness is uniform and that the radial stress is not considered.[21] In addition to this, there are other assumptions considered to simplify the model:

1. Axial symmetry of the shell: All variables are independent from θ ($\tau_{\theta r} = \tau_{r\theta} = \tau_{z\theta} = \tau_{\theta z}$).
2. Plane state of stress: Stress in the thickness direction is negligible ($\sigma_{rr} = 0$, $\tau_{zr} = \tau_{rz} = 0$, $\tau_{\theta r} = \tau_{r\theta} = 0$).
3. No friction between the wedge and the shell: The force applied locally is transferred homogeneously all over the shell.
4. Transverse cracks are neglected: Shear force created by the wedge is ignored.

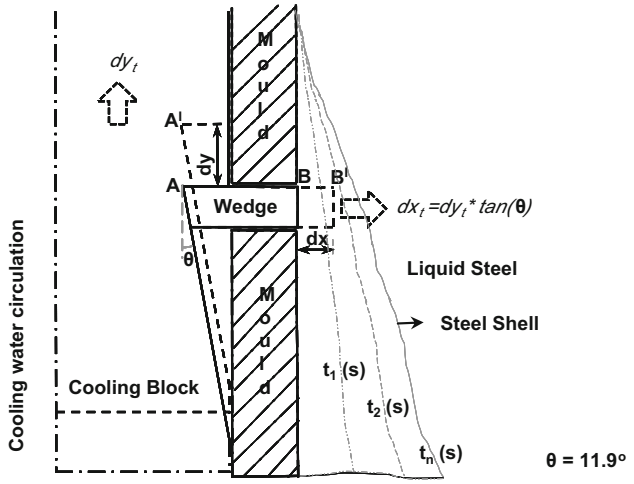

Fig. 4—Schematic view of cooling block and wedge assembly inside the mold.

A. *Calculation of Strain*

During deformation, the cooling block is pulled in the longitudinal direction. Due to slide motion between the inclined plane on the cooling block and the wedge, the load and displacement are transferred to the wedge, which are then transmitted to the solidified shell formed on the mold surface.

Figure 4 shows the movement of the assembly with respect to the incremental displacement dy. When the inclined plane moves dy in positive longitudinal direction, *i.e.*, upwards from A to A^I, the wedge moves dx in radial direction from B to B^I.

Therefore, dx can be calculated from the measured dy using Eq. [1].

$$dx_t = dy_t * \tan(\theta) \quad [1]$$

Upon the assumption that the solidified shell can be treated as a circular cylindrical body of annular cross section, the true strain $\varepsilon_{\theta\theta}$ is defined as follows:

$$\varepsilon_{\theta\theta} = \ln\left(\frac{\text{Circumference of the shell}_{(t)}}{\text{Initial circumference}}\right). \quad [2]$$

During the displacement dy_t, a gap of magnitude dx_t is formed on both sides between the mold and wedge . Therefore, the inner circumference of the shell at time t is the sum of initial circumference and twice the gap formed between mold and wedge dx_t. Substituting into Eq. [2] yields the following:

$$\varepsilon_{\theta\theta} = \ln\left(\frac{(\pi * d_{\text{mold}}) + (2 * dx_t)}{(\pi * d_{\text{mold}})}\right) = \ln\left(1 + \frac{2 * dx_t}{\pi * d_{\text{mold}}}\right), \quad [3]$$

where d_{mold} denotes the diameter of the mold (69.36 mm) and 2*dx_t is the increase in circumference at time t during deformation. It is obvious that the strain is strongly affected by dx_t, which is determined by Eq. [1].

The strain rate being the change in strain with respect to time can be calculated thus [4]:

$$\dot{\varepsilon} = \frac{d\varepsilon_{\theta\theta}}{dt} = \frac{d}{dt}[\ln(1 + (0.009178 * dx_t))]. \quad [4]$$

For these tests, the strain rate has been calculated to be 0.008 to 0.010 (1/s).

B. *Calculation of Stress*

The force applied by the load cell in the longitudinal direction is not completely transmitted onto the shell. Due to sliding action between the inclined plane (on the cooling bock) and wedge, only a part of the force applied by the hydraulic cylinder is transmitted by the wedge, which can be calculated by the resolving forces along the inclined surface as shown in Figure 5 and explained here further.

The force F applied on the cooling block during deformation can be resolved into a normal force perpendicular to the incline plane F_N and the sliding force F_S along the inclined plane. The normal force exerted perpendicular to the incline plane on to the wedge is calculated by Eq. [5].

$$F_N = F * \sin(\theta). \quad [5]$$

The normal force F_N can further be resolved into forces acting in horizontal direction and transverse direction F_w, F_T, respectively. The force exerted by the wedge F_w on the solid shell is calculated by Eq. [6].

$$\begin{aligned} F_w &= F_N * \cos(\theta) \\ F_w &= F * \sin(\theta) * \cos(\theta) \end{aligned}. \quad [6]$$

Since the friction coefficient μ between various moving parts in the assembly, *i.e.*, between inclined surface and wedge is not known and may be a function of temperature, it is included in the overall force measured. During every MCS experiment, the apertures are made idling, *i.e.*, the simulator is operated without the liquid metal (here called "cold test"). The difference between force measured (ΔF) in the hot test (with liquid metal) and in the cold test gives the amount of force transmitted onto the wedge by subtracting the force lost due to friction and weight of the tool itself (Figure 6). However, this approximation has limitations because the cold test is carried out at room temperature and the hot test with liquid steel at high temperature. A temperature-dependent friction coefficient is, therefore, a potential source of error.

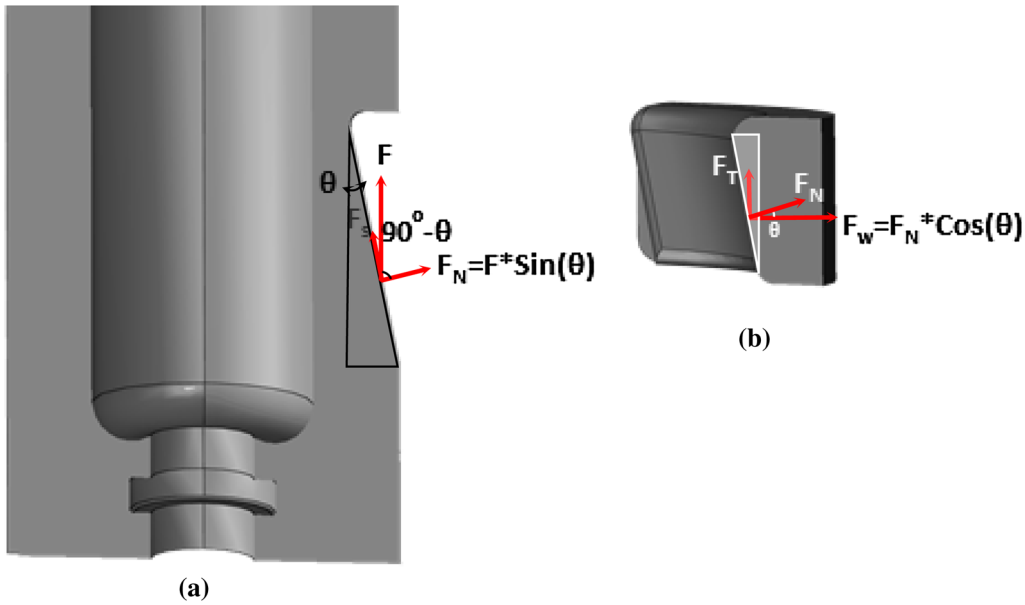

Fig. 5—Resolution of forces along the inclined plane: (*a*) cooling block, (*b*) wedge.

Replacing F with ΔF and subsuming $\theta = 11.9$ in Eq. [7],

$$F_w = \Delta F * 0.1954. \quad [7]$$

Thus only 19.54 pct of the load applied on the cooling block is transmitted by the wedge onto the solidifying shell.

Since the thin wall assumption is used, the circumferential and longitudinal stresses are considered to be constant across the wall thickness, and because the magnitude of the radial stress is small in comparison with the hoop and longitudinal stresses, it can be neglected.

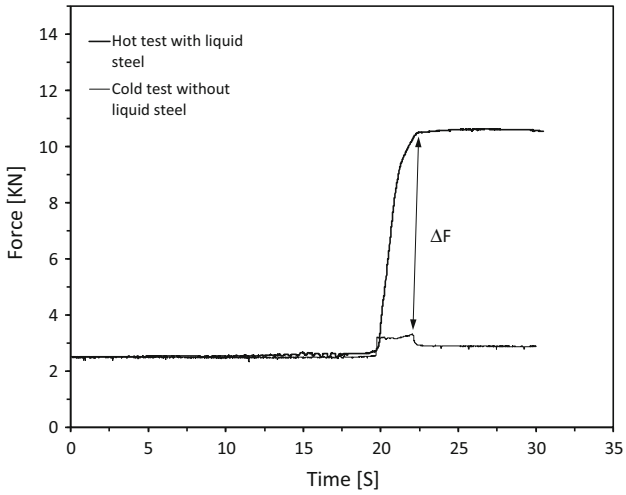

Fig. 6—Force observed during hot and cold tests.

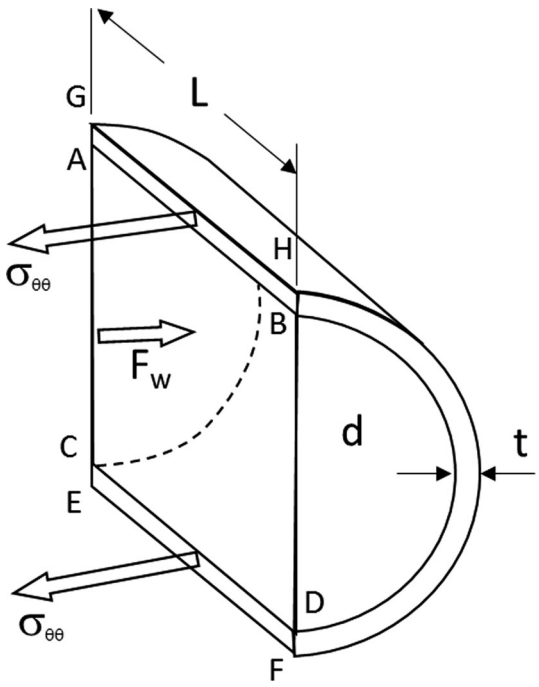

Fig. 7—Schematic view of half cut solidified shell.

The internal pressure applied by the wedge F_w on the solid shell (on plane ABCD in Figure 7) is transferred as a circumferential stress, acting on the planes ABHG and CDFE as shown in Figure 7. The total resisting force owing to hoop stress on the cylinder walls (on the planes ABHG and CDFE) equals to the stress on the walls multiplied with the corresponding area of the walls. Therefore, F_w will be

$$F_w = 2\,\sigma_{\theta\theta} * (L * t). \quad [8]$$

Substituting, $F_w = 0.1954*\Delta F$ from Eq. [8], the hoop stress is:

$$\sigma_{\theta\theta} = \frac{\Delta F * 0.1954}{2 * L * t}. \quad [9]$$

Grouping all constants, the hoop stress can be calculated by

$$\sigma_{\theta\theta} = \frac{4.9095 * \Delta F}{t}\ (\text{MPa}). \quad [10]$$

IV. RESULTS AND DISCUSSION

Two steel grades (chemical composition given in Table I) were chosen for testing and assessment of the mechanical state with the mathematical model described here, to translate the measured force and elongation into stress–strain data.

Four tests, two for each of the two different steel grades were performed using MCS. During the test, the mold temperature was recorded with two type K shielded thermocouples. The inlet and outlet cooling water temperature, as well as the water flow were measured for calculation of the heat flux. Load and displacement were recorded throughout the test. All signals were acquired *via* a data-logging system. Temperature signals were logged at a frequency of 50 Hz (20 ms) and the other signals at 200 Hz (5 ms).

After testing, the shell solidified around the mold was taken for metallographic analysis. For the true stress–true strain calculation, it is necessary to acquire an accurate value of the shell thickness. For this reason, 3D measurements of the shell thickness were made in accordance with a method used for breakout shell thickness analysis.[22] An example of this measurement is in Figure 8 for steel 1. At the right-hand side of Figure 8, the thickness of the shell is shown for the position at the red-white dotted line. On the left-hand side, the image shows that the thickness is rather constant along the whole shell, ranging from 1 mm at the top (meniscus) to 2 mm at the bottom; however, some fluctuations are seen as expected, particularly at the areas with oscillation marks.

Table I. Chemical Composition of the Melt During MCS Experimental Trials

(Wt. Pct)	C	Si	Mn	S	Cu	Cr	Mo	Ni	Nb	N	(T_L)	(T_S)
Steel-1	0.13	—	0.1	0.005	—	—	—	0.02	—	—	1799 K (1526 °C)	1763 K (1490 °C)
Steel-2	0.28	0.24	1.3	0.004	0.34	1.3	0.5	0.03	0.04	0.02	1779 K (1506 °C)	1712 K (1439 °C)

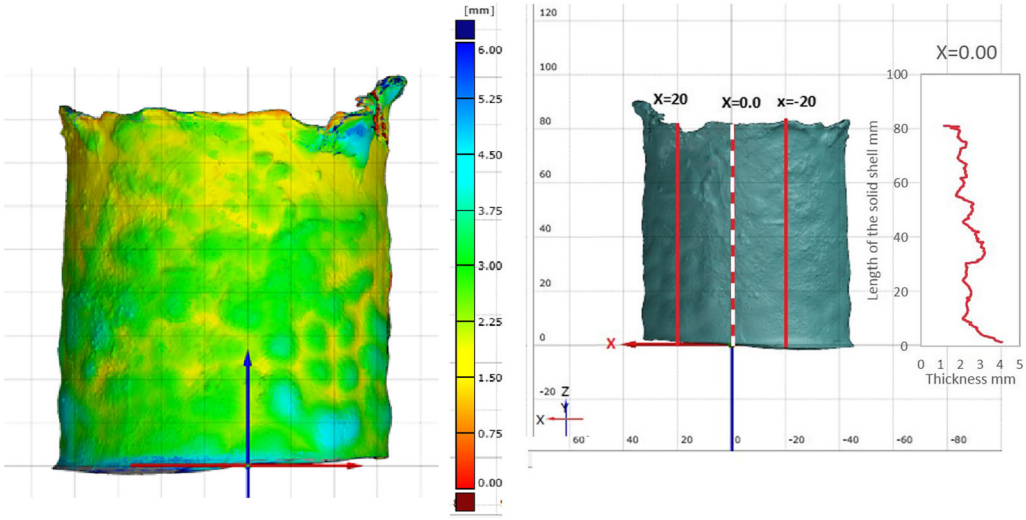

Fig. 8—3D shell thickness scan for steel-1. Left: 3D shell thickness scan. Right: shell thickness measured at position $x = 0.0$.

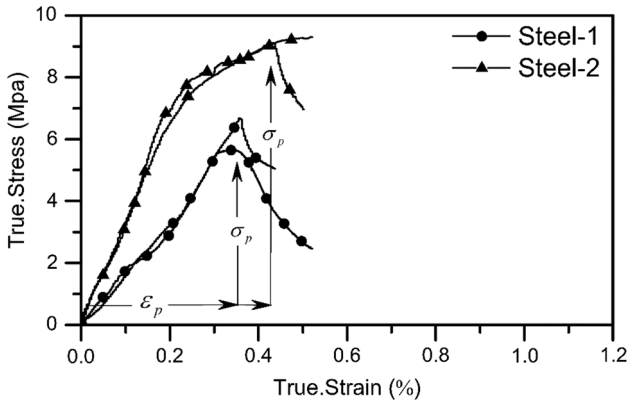

Fig. 9—Stress–strain results for steel 1 and 2.

A. *Stress–Strain Curves*

Out of four tests performed, a good reproducibility has been observed between the same steel grades. Figure 9 shows the stress–strain curves for the two grades considered in this study.

Considering that the chemical composition of both steels is different, expectedly, their mechanical state during solidification should be also dissimilar. A first indication of cracking susceptibility of a steel grade under testing conditions can be seen by the maximum stress σ_p, and its corresponding strain ε_p, considering that this point is the ultimate tensile strength (UTS).

The steel-2 with higher amount of alloying elements showed better mechanical properties ($\sigma_p \approx 9$ MPa and $\varepsilon_p \approx 0.45$ pct) both in terms of strength and ductility, when compared to steel-1 ($\sigma_p \approx 6$ MPa and $\varepsilon_p \approx 0.35$ pct). The maximum applied strain during testing exceeds 0.6 pct in all the four cases; however, the samples were already cracked before reaching this point. These values are comparable with various other similar published results.[6,23,24]

B. *Metallographic Analysis*

Considering that one of the design objectives of the MCS test was to obtain thermomechanical data for steel under solidification conditions, in particular to be used to assess the hot tearing susceptibility; this implies that the induced cracks should be interdendritic of nature.

All samples do crack longitudinally, *i.e.*, parallel to the casting direction and thus, against the oscillation marks. All shells do have one single big crack. When more than one crack is seen on the shell, it is obvious that one of them is larger than the others.

The steel shells were cut on the transverse direction, perpendicular to the main crack direction, polished and etched with Bechét–Beaujard etchant.

The dendritic microstructure of the MCS steel shells is comparable to the microstructure of a continuously cast steel. Because steel-2 is a higher-alloyed grade, it shows a finer dendritic structure compared to the lower-alloyed steel (steel-1). The micrographs showing dendritic structures of both steels are presented in Figure 10. The measured dendrite arm spacing (Figure 11) likewise supports these observations.

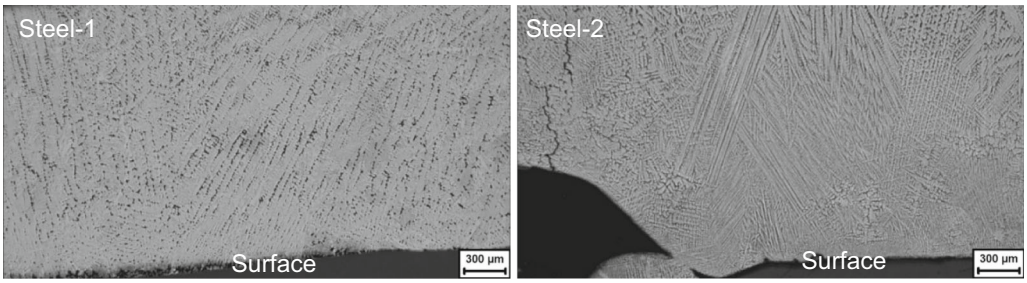

Fig. 10—Dendritic morphology of steel 1 and 2.

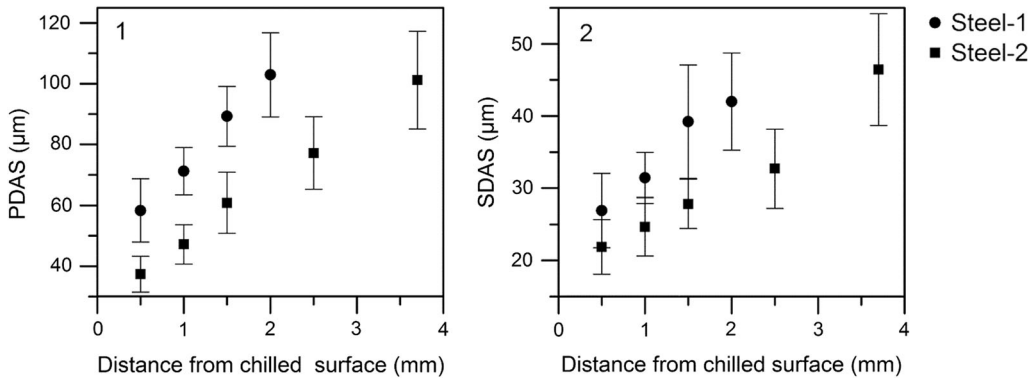

Fig. 11—Dendrite arm spacing's (1) Primary Dendrite Arm Spacing (PDAS); (2) Secondary Dendrite Arm Spacing (SDAS).

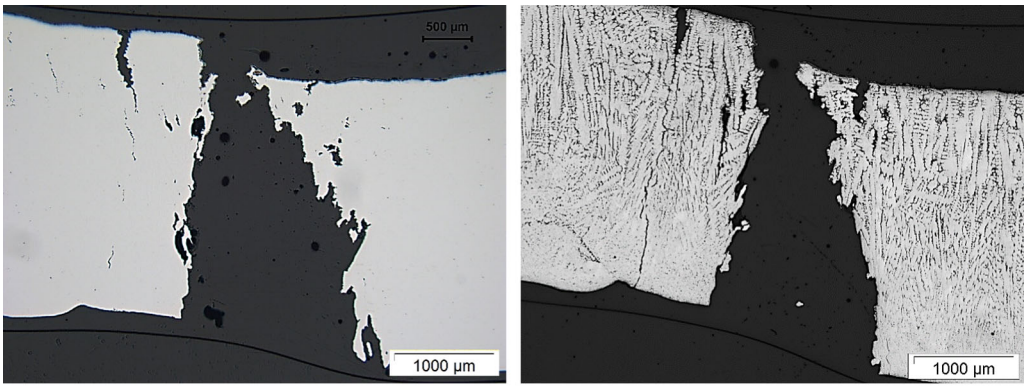

Fig. 12—Cross-sectional view of fracture surface of Steel-2: (*a*) polished surface, (*b*) Bechét–Beaujard etched.

In steels with higher alloy content, the segregating ability of solute elements restricts the growth of solid–liquid interface by reducing the rate of diffusion, leading to a significant grain refinement.[25] Moreover, the constitutionally undercooled zone in front of the interface also increases the possibility for perturbations (new nuclei) to grow and subsequently affects the growth of the preceding ones.[26,27]

A refined dendritic structure is well known to improve mechanical properties. Especially, secondary dendrite arm spacing (SDAS) λ_2 affects the permeability and coalescence of semisolid structures during solidification which, in turn, affects the hot tearing susceptibility of an alloy,[23,25] increasingly fine dendrites having increasingly more contact area with the adjacent dendrites, thus requiring more force to tear them apart. In the present study, two steel grades with different alloy contents were taken into account. One possible reason for the higher strength of steel-2 during solidification is its high coalescence between the dendrite arms when compared to the lower-alloyed steel having coarser dendritic structure.

Figure 12 shows polished and etched cross-sectional view of the fractured surfaces. The micrographs show

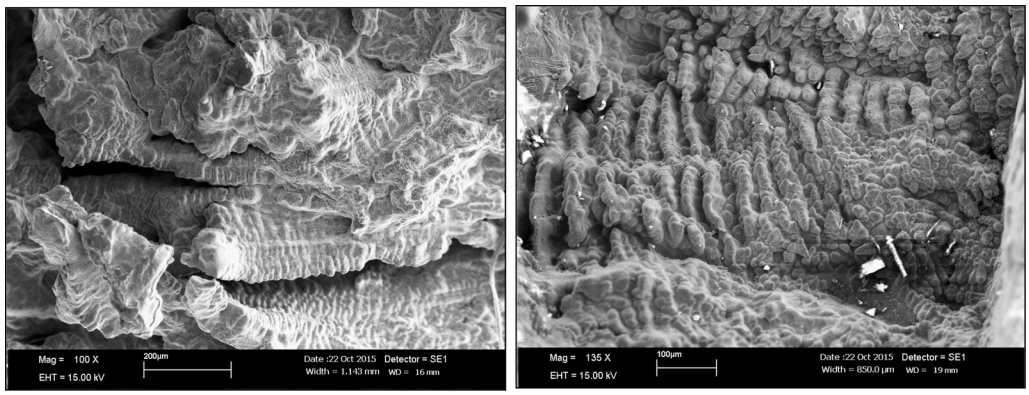

Fig. 13—Overview of the fracture surfaces of Steel-2.

that the dendritic structure was ripped apart during the deformation. Many interdendritic cracks are visible over the whole length of the specimen.

Because the shells have been ruptured along the thickness, it can be considered that the strain distribution is uniform along the circumferential direction in the shell.

For a more complete analysis of the cracks, fractography has been performed at the fracture surface. The fractured surfaces were observed and evaluated under the Scanning Electron Microscope (SEM) at Tata Steel R&D IJTC (IJmuiden Technology Centre) and Steel Institute IEHK of RWTH Aachen University. The dendrite arm network of dendrites arms was observed on the fracture surfaces, thereby confirming that the cracks are interdendritic. In some parts of the samples, the fracture surfaces are partially covered by mold slag which wets the surface of the formed shell upon its removal from the MCS mold after solidification. When the deformation occurs out of the bath, it is expected that a small amount of slag penetrates the fracture surface as it is still hot and not yet solidified. However, the dendritic structure is visible in most of the areas. In Figure 13, an example of the fractured surface of steel 2 is shown.

Combining that temperatures measured by the two mold thermocouples are comparable to the expected values at the gap between the steel shell and the mold at the early stages of solidification,[28] and the fractographic analysis, it can be assumed that the test is suitable for assessment of the mechanical state of a steel during solidification.

V. CONCLUSIONS AND OUTLOOK

In the present work, a model has been developed to determine true stress–true strain curves for steels during solidification with the Mold Crack Simulator (MCS).

The mathematical model presented is based on the thin wall assumption since the test piece is a circular cylindrical body of annular cross section subjected to surface forces and thermal loads.

Two steel grades were used for testing and validation of such a model and the reproducibility of the results is very good. The higher-alloyed steel grade showed better mechanical properties, both in terms of strength and ductility, when compared to the other steel grade, most likely due the finer dendrite structure of that steel resulting in increased load-bearing capacity.

The metallographic analysis of the solidified shells showed that the dendritic microstructure is comparable to a continuously cast product.

Combining the results of the fractography and metallographic analysis indicate firstly, that the strain distribution is uniform along the circumferential direction in the shell; secondly, that the cracks are interdendritic in nature, thus suitable to mimic cracking at the early stages of solidification; and thirdly, that the test is suitable for assessment of the mechanical state of a steel during solidification.

Further experimental investigations are needed using MCS to study the strength of different steel grades during solidification .A comparison with already published similar results needs to be done as well, whenever possible, considering that the testing conditions of the few similar devices available up to now differ considerably.

LIST OF SYMBOLS

T_S	Solidus temperature (°C)
T_L	Liquidus temperature (°C)
L	Length of the wedge (19.9 mm)
d_{mold}	Diameter of the mold (69.36 mm)
θ	Angle of the curved inclined surface
R	Radius of solidified shell in (mm)
t	Thickness of the solidified shell in (mm)
F_N	Normal force perpendicular to the incline plane (N)
F_w	Load transmitted by wedge on to the shell (N)

F_S	Sliding force along the inclined plane (N)
ΔF	Difference between forces measured during hot test and cold test (N)
dy	Incremental displacement in positive longitudinal direction, *i.e.*, from A to A^I
dx	Incremental displacement in radial direction from B to B^I (refer Figure 4)
$\dot{\varepsilon}$	Strain rate, change in strain of a material with respect to time (1/s)
σ_p	Peak stress (MPa)
$\dot{\varepsilon}_p$	Strain at Peak stress (pct)
$\varepsilon_{\theta\theta}$, ε_{rr}, and ε_{zz}	Normal strains measured along the radial, tangential, and axial directions, respectively (elongation/ shortening of material per unit length)
$\sigma_{\theta\theta}$, σ_{rr}, and σ_{zz}	Normal stress along the radial, tangential, and axial directions, respectively (force per unit area)
$\tau_{\theta\theta}$, $\tau_{\theta z}$, and τ_{zr}	Shear stress, components of stress coplanar with a material cross section (force per unit area)

REFERENCES

1. K.O. Yu, ed., *Modelling for casting and solidification processing*, vol. 1. New York: Marcel Dekker, 2009.
2. W.T.J. Lankford: *Metall. Trans.*, 1972, vol. 3, pp. 1331–56.
3. H. Mizukami, A. Yamanaka, and T. Watanabe: *ISIJ Int.*, 2002, vol. 42 (9), pp. 964–73.
4. T. Nakagawa, T. Umeda, J. Murata, and Y. Kamimura: *ISIJ Int.*, 1995, vol. 35 (6), pp. 723–29.
5. B. Mintz, J.R. Wilcox, and D.N. Crowther: *Mater. Sci. Technol.*, 1986, vol. 2 (6), pp. 589–94.
6. C. Bernhard, H. Hiebler, and M.M. Wolf: *ISIJ Int.*, 1996, vol. 36, pp. 163–66.
7. H. Presslinger *et al.*: *ISIJ Int.*, 2006, vol. 46 (12), pp. 1845–51.
8. H. Yasunaka, T. Mori, H. Nakata, F. Kamei, and S. Harada: *Steelmak. Process.*, 1986 (69), pp. 497–502.
9. H.G. Suzuki, S. Nishimura, and Y. Nakamura: *Trans. Iron Steel Inst. Jpn.*, 1984, vol. 24 (1), pp. 54–59.
10. B Rogberg: *Scand. J. Metall.*, 1983, vol. 12, pp. 51–66.
11. K. Hansson: Ph.D. Thesis, Royal Institute of Technology, Stockholm, Sweden, 2001.
12. T.T. Natarajan, T.J. Piccone, K.D. Powers, C.C. Snyder, A. Badri, and A.W. Cramb: *AISTech2004*, 2004, vol. II, pp. 1013–25.
13. P. Kozlowski, B.G. Thomas, J. Azzi, and H. Wang: *Metall. Trans. A*, 1992, vol. 23A, pp. 903–18.
14. H. Zhang, Y. Wang, and W. Zhang: *Metall. Mater. Trans. B*, 2016, vol. 47B, pp. 2244–52.
15. P. Ackermann, W. Kurz, and W. Heinemann: *Mater. Sci. Eng.*, 1985, vol. 75 (1), pp. 79–86.
16. C. Bernhard, R. Pierer, and S. Michelic: *AISTech*, 2010, pp. 977–86.
17. B. Santillana and M. Cruijff: WO patent request, 2011.
18. G.E. Dieter: *Mechanical Metallurgy*, McGraw-Hill Book Co, New York, 1998, vol. SI metric.
19. B. Santillana, B.G. Thomas, A. Hamoen, L.C. Hibbeler, A. Kamperman, and W. Van Der Knoop, *AISTech - Iron and Steel Technology Conference Proceedings*, 2007, vol. 2, CD-Rom.
20. B.G. Thomas, A. Moitra, and H. Zhu, *Miner. Met. Mater. Soc.* 1995, pp. 240–49.
21. V. Vullo: *Circular Cylinders and Pressure Vessels. Stress Analysis and Design*, Springer, Berlin, 2014.
22. B. Santillana, B.G. Thomas, G. Botman, and E. Dekker: in *7th European Continuous Casting Conference*, 2012.
23. T. Suzuki, C.H. Yu, and T. Emi: *ISIJ Int.*, 1997, vol. 37 (4), pp. 375–82.
24. C. Bernhard, H. Hiebler, and M.M. Wolf: *La Rev. Metallurgie*, 2000, pp. 333–43.
25. L. Arnberg and R.H. Mathiesen: *JOM*, 2007, vol. 59 (8), pp. 20–26.
26. B. Santillana: Ph.D. Thesis TU Delft, 2013.
27. M. Easton and D. Stjohn: *Metall. Mater. Trans. A*, 2005, vol. 36A (7), pp. 1911–20.
28. Y. Meng and B.G. Thomas: *Metall. Mater. Trans. B*, 2003, vol. 34B, pp. 707–25.